Journal of Photochemistry & Photobiology, A: Chemistry 412 (2021) 113220

Contents lists available at ScienceDirect

Journal of Photochemistry & Photobiology, A: Chemistry

journal homepage: www.elsevier.com/locate/jphotochem

Fluorescence and phosphorescence of α- and β-isomers of boron Difluoride naphthaloylacetonates

Elena V. Fedorenko [a,*], Anatolii G. Mirochnik [a], Andrey V. Gerasimenko [a], Anton Yu. Beloliptsev [a], Zakhar N. Puzyrkov [a,b], Irina V. Svistunova [b], Aleksander A. Sergeev [c]

[a] Institute of Chemistry, Far Eastern Branch, Russian Academy of Sciences, 159, Prosp. 100-letiya Vladivostoka, Vladivostok, 690022, Russian Federation
[b] Far Eastern Federal University, 8, Sukhanova Str., Vladivostok, 690950, Russian Federation
[c] Institute of Automatics and Control Processes, Far East Branch, Russian Academy of Sciences, Vladivostok, 690041, Russian Federation

ARTICLE INFO

Keywords:
Luminescence
Phosphorescence
Boron difluoride β-diketonates
Excimer

ABSTRACT

A comparative study of the luminescence properties of solutions and crystals of two isomers: boron difluoride 1-(1′-naphthyl)butanedionate-1,3 (α-NAcBF$_2$) and 1-(2′-naphthyl)butanedionate-1,3 (β-NAcBF$_2$) has been performed. An interrelation between the molecular and crystal structure of the studied complexes and their luminescence properties has been revealed. In the α-NAcBF$_2$ molecule, the plane of the naphthyl group was turned by 34.26° relatively to the chelate cycle, while the β-NAcBF$_2$ molecule was planar. The difference in the luminescence properties of the crystals of α-NAcBF$_2$ (452 nm) and β-NAcBF$_2$ (537 nm) was related to different abilities to form excimers. In β-NAcBF$_2$ crystals, J-aggregates consisted of dimers of antiparallel molecules comprising excimer traps. For the crystals and solutions of α-NAcBF$_2$ at 77 K, in addition to phosphorescence, the delayed fluorescence was observed. In case of β-NAcBF$_2$, the delayed fluorescence was detected only for crystals, whereas the phosphorescence – for both crystals and solutions.

1. Introduction

Fluorescent dyes are subject to the constant attention of researchers in various fields and important applications in various areas: conversion of solar energy, organic electronics, visualization, creation of fluorescent labels, probing, and as biomaterials in medical diagnostics and photodynamic therapy [1–8]. As can be seen from numerous studies on boron dipyrromethene dyes (BODIPY) [9–13], tetra-coordinated boron complexes were of the most important. Here, the most valuable properties of luminophores include stability, high absorption coefficients and quantum yields of fluorescence, and high Stokes shifts, which is not always typical for BODIPY dyes. Various types of BF_2 fluorescent complexes were recently synthesized as an alternative to BODIPY, including β-diketoiminates [14–16], β-ketoiminates [17–20], and β-diketonates [21–24]. β-Diketonates of boron difluoride were of particular interest, since they exhibited an intensive luminescence both in solutions and in the solid state, which was determined by molecular and supramolecular architecture. The electron-acceptor properties of BF_2 and the structural features of diketonate fragments led to intermolecular interactions of various natures (π-stacking, hydrogen bonds, van der Waals and energy donor-acceptor interactions, etc.), resulting in self-organization and the formation of excimers and exciplexes [25–30]. There are many examples of the effect of the molecular design of a β-diketonate ligand on the emission properties of complexes. For example, the introduction of various aromatic groups (phenyl, naphthyl, and anthracyl) can affect the wavelength of radiation [31], whereas the halide substitution can effectively affect the intensity of fluorescence [32]. The combination of aromatic groups with different halide substitutes allow controlling the luminescent properties [33–35]. On the other hand, substituents of the same type might not change the emission properties of dilute solutions, but significantly affect their intermolecular organization and, accordingly, the luminescence of aggregates in concentrated solutions and crystals [36–38].

Even minor variations in the molecular structure, such as the position of the substituent or its isomerization, change the crystal packaging and optical properties of compounds, which can have a key role in the development of functional optical materials of a new type [39–42]. Therefore, revealing factors that affect the luminescent properties of boron chelates is of urgent importance.

In the present work, a comparative study of the luminescent

* Corresponding author.
E-mail address: gev@ich.dvo.ru (E.V. Fedorenko).

https://doi.org/10.1016/j.jphotochem.2021.113220
Received 12 November 2020; Received in revised form 19 February 2021; Accepted 20 February 2021
Available online 25 February 2021
1010-6030/© 2021 Published by Elsevier B.V.

properties of solutions and crystals of two isomers was performed: boron difluoride 1-(1′-naphthyl)butanedionate-1,3 (β-NAcBF$_2$) and 1-(2′-naphthyl)butanedionate-1,3 (β-NAcBF$_2$) (Scheme 1).

2. Experimental

2.1. Materials

Chloroform, benzene, dichlormethane, and carbon tetrachloride were purchased from Roskhimreaktiv company and used as received. Boron trifluoride (acetic acid complex) was purchased from the Acros Organics and used as received. Acetic anhydride was purified by distillation with a reflux condenser. 1- and 2-acetonaphthones were synthesized according to [43].

2.1.1. Boron difluoride 1-(1′-naphthyl)butanedionate-1,3 (α-NAcBF$_2$)

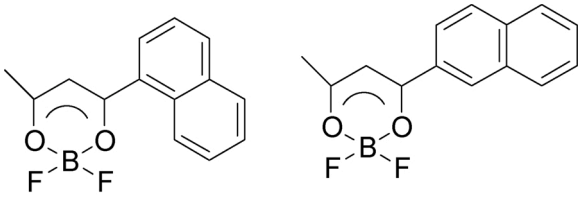
A solution of 1.09 g of α-acetonaphthone in 3 ml acetic anhydride was added to a mixture of 1.78 ml BF_3·2(CH_3COOH) and 5 ml of acetic anhydride at 45 °C for 6 h. After, the mixture was stirred for another 3 h. Mixture was cooled, the precipitate was filtered and washed with acetic acid. Yield equaled to 0.89 g (54 %). Recrystallized from acetonitrile (50 %). M. p. 153−154 °C, $R_f = 0.40$ (chloroform: hexane 1:2). ^{1}H NMR 400 MHz ($CDCl_3$), δ/ppm: 2.43 (s, 3 H) 6.48 (s, 1 H) 7.49–7.66 (m, 3 H) 7.88–7.94 (m, 2 H) 8.08 (d, $J = 8.19$ Hz, 1 H) 8.48 (d, $J = 8.68$ Hz, 1 H). ^{13}C NMR 100 MHz ($CDCl_3$), δ/ppm: 24.75 (s, 1C), 76.67 (s, 1C), 76.99 (s, 1C), 77.19 (s, 1C), 77.31 (s, 1C), 102.07 (s, 1C), 124.56 (s, 1C), 125.11 (s, 1C), 127.02 (s, 1C), 128.56 (s, 1C), 128.90 (s, 1C), 129.89 (s, 1C), 130.20 (s, 1C), 133.84 (s, 1C), 134.97 (s, 1C), 186.96 (s, 1C), 192.45 (s, 1C). IR (KBr), ν/cm^{-1}: 3145, 3062 (C-H_{Ar}), 1627 ($C_{10}H_7$), 1598, 1541 (C = O, C = C), 1373 (B–O), 1184 1155 (B–F), 1078, 1053 (B–O). Anal. calc. for $C_{14}H_{11}BF_2O_2$: C 64.66 %, H 4.26 %, Found: C 64.45 %, H 4.22 %.

2.1.2. Boron difluoride 1-(2′-naphthyl)butanedionate-1,3 (β-NAcBF$_2$)

A solution of 0.425 g β-acetonaphthone in 2 mL acetic anhydride was added to a mixture of 0.7 ml BF_3·2(CH_3COOH) and 3 ml of acetic anhydride at a temperature of 45 °C for 6 h. After, the mixture was stirred for another 3 h. Mixture was cooled, the precipitate was filtered and washed with acetic acid. Yield equaled to 0.73 g (81 %). Recrystallized from acetonitrile (59 %). M. p. 182−183 °C, $R_f = 0.33$ (chloroform: hexane 1:2). ^{1}H NMR 400 MHz ($CDCl_3$), δ/ppm: 2.46 (s, 3 H) 6.73 (s, 1 H) 7.57–7.71 (m, 2 H) 7.88–8.04 (m, 4 H) 8.70 (d, $J = 0.98$ Hz, 1 H). ^{13}C NMR 100 MHz ($CDCl_3$), δ/ppm: 24.79 (s, 1C), 97.66 (s, 1C), 123.36 (s, 1 C), 127.46 (s, 1C), 127.89 (s, 1C), 128.26 (s, 1C), 129.07 (s, 1C), 129.88 (s, 1C), 129.96 (s, 1C), 131.81 (s, 1C), 132.42 (s, 1C), 136.56 (s, 1C), 182.62 (s, 1C), 192.16 (s, 1C).). IR (KBr), ν/cm^{-1}: 3145, 3064 (C-H_{Ar}), 1627 ($C_{10}H_7$), 1598, 1542 (C = O, C = C), 1373 (B–O), 1184 1153 (B–F), 1078, 1049 (B–O). Anal. calc. for $C_{14}H_{11}BF_2O_2$: C 64.66 %, H 4.26 %, Found: C 64.40 %, H 4.28 %.

2.2. Measurements

For spectra measurements, diluted solutions of an optical density of 0.1 (C = 1.7·10^{-5} mol L^{-1}) and concentrated solutions (C = 2.6·10^{-3} mol L^{-1}) were used.



α-NAcBF$_2$ β-NAcBF$_2$

Scheme 1. Chemical structure α-NAcBF$_2$ and β-NAcBF$_2$.

The absorption spectra were registered using a Shimadzu-UV2550 spectrometer (Japan) in cells of a size of 10 × 10 mm. Luminescence and excitation spectra were registered using a Shimadzu-RF5301 spectrometer (Japan). The spectra of the diluted solutions were registered in a cell of a size of 10 × 10 mm with standard cell positioning. The spectra of the concentrated solutions were registered in a cell of a size of 10 × 1 mm with frontal cell positioning. Excitation and emission spectra were recorded on crystals using the front-face configuration of the spectrofluorimeter. A solution of anthracene in ethanol was used as a standard for measuring the fluorescence quantum yield (ϕ = 0.27). The measurements of the fluorescence lifetime by time-correlated single-photon counting (TCSPC) were performed using a FluoTime 200 device (PicoQuant, Germany) with a LDH-P-C-375 (370 nm, pulse wide 6 ns and repetition rate 20 MHz) excitation source and a TimeHarp device as the SPC controller.

Fluorescence, phosphorescence and excitation spectra at 77 K were registered using a spectrofluorimeter Fluorolog 3 (Horiba) using a cryostate. Phosphorescence spectra were recorded under excitation maxima of 350 and 370 nm for α-NAcBF$_2$ and β-NAcBF$_2$, respectively. Excitation pulse was 50 ms long, data collection started at 0.5 ms after pulse with a 0.2 ms sample window.

IR spectra were recorded using a HEWLETT PACKARD Series 1110 MSD spectrometer in potassium bromide. NMR spectra were recorded using an Avance 400 MHz high resolution spectrometer (Bruker) on ^{1}H, ^{13}C nuclei at different operating frequencies. The melting point of the substances synthesized in the present study was determined using a Büchi melting point model B-540 instrument.

2.3. Computational details

Quantum chemistry simulation of electronic absorption spectra of α-NAcBF$_2$ and β-NAcBF$_2$ was carried out using the GAMESS-US software complex [44]. The compounds structural parameters, energy characteristics, and electronic structure were determined at complete geometry optimization in the 6−311 G(d, p) basis by the nonempirical method and the density functional theory with the exchange-correlation potential B3LYP [45]. Electronic absorption spectra of compounds with taking into account excited singlet states were calculated by the TDDFT method in the 6−311 G(d, p) basis with the B3LYP potential. Effects from various solvents were also taken into account using the polarizable continuum model (PCM). The positions of the maxima of luminescence spectra were calculated as the energy of transition between S_0' and S_1' in the optimized geometry of the first excited state. A comparative study of the structure of the boundary orbitals, the order of transitions, and the values of the forces of the band oscillators in the absorption spectra during the transition from the vacuum approximation to the molecule in the electromagnetic field of the solvent showed no significant differences (Table 1S). Therefore, only the vacuum approximation was used to explain the differences in the experimental spectra of the α-NAcBF$_2$ and β-NAcBF$_2$ isomers.

2.4. X-ray crystallographic analysis

Experimental data for α-NAcBF$_2$ were collected using a BRUKER Kappa APEX II diffractometer. The intensity data were corrected for absorption using the multi-scan method.

The structure was determined using direct methods and refined by least-squares calculation in anisotropic approximation for non-hydrogen atoms. Hydrogen atoms were added at ideal positions and refined using a riding model. The data collection and editing, as well as refinement of unit cell parameters, were performed using the APEX2 program packages [46]. The structure solution and refinement were performed using the SHELXTL program packages [47,48].

Crystal data for α-NAcBF$_2$ ($C_{14}H_{11}BF_2O_2$): Pale yellow needles, 0.386 × 0.341 × 0.044 mm^3, monoclinic, Pc, $a = 10.3165(4)$,

$b = 7.4968(3)$, $c = 8.6257(3)$ Å, $\alpha = 90°$, $\beta = 113.542(2)°$, $\gamma = 90°$, V = 611.59(4) Å^3, Z = 2, $\rho_{calc} = 1.412$ Mg/m^3, $\mu = 0.112$ mm^{-1}, $Mo_{K\alpha}$ radiation (λ =0.71073 Å), T = 296(2) K, $2\theta_{max} = 50.484°$, 9434 reflections measured, 3055 unique reflections, $R_{int} = 0.0301$, 268 parameters, for $I > 2\sigma(I)$ R1 = 0.0395, wR2 = 0.0877; for all data R1 = 0.0694, wR2 = 0.1012. CCDC 1989898.

The structure of β-NAcBF$_2$ was defined in [49] CCDC 721686.

3. Results and discussion

3.1. Synthesis of α-NAcBF$_2$ and β-NAcBF$_2$

In [49], acylation of naphthalene was performed with acetic anhydride and gas boron trifluoride to synthesize boron difluoride 1-(2′-naphthyl)butanedionate-1,3. However, the reaction was highly exothermic and inexact maintenance of temperature conditions led to the formation of a large amount of intensely colored by-products. Acylation of a number of aromatic compounds under milder conditions with acetic anhydride and boron trifluoride diacetate was described in [50]. Acylation of naphthalene under similar conditions resulted in the formation of a difficult-to-separate mixture of α-NAcBF$_2$ and β-NAcBF$_2$ (Fig. 7S).

Individual α-NAcBF$_2$ and β-NAcBF$_2$ were prepared by acylation of 1- and 2-naphthylmethyl ketones with acetic anhydride and boron trifluoride diacetate (Scheme 2). 1- and 2-naphthylmethyl ketones were prepared by acylation of the naphthalene by acetylchloride with aluminum chloride in dichloroethane (1-acetonaphthone) and nitrobenzene (2-acetonaphthone) [43].

3.2. Molecular structures of α-NAcBF$_2$ and β-NAcBF$_2$

The calculated geometry of isomeric naphthaloylacetonates of boron difluoride was in good agreement with the experimental one (Table 1). The corresponding bond lengths of both isomers were proximate to each other, both calculated and experimental ones.

The difference in the structure of the isomers α-NAcBF$_2$ and β-NAcBF$_2$ consisted in the fact that in the α-NAcBF$_2$ molecule the plane of the naphthyl group was turned by 34.26° relatively to the chelate cycle, while the β-NAcBF$_2$ molecule was virtually plane, and the turning angle of the naphthyl group was as small as 2.13°. This was the result of the repulsion of hydrogen atoms in the β-NAcBF$_2$ molecule near a central carbon atom of the chelate cycle (H(2)) and in the β-position of the naphthyl group (H(6)) (Fig. 1). One also observes a repulsion between the H(13) and O(1) atoms, which contributes to the twisting of the α-NAcBF$_2$ molecule. In both cases, the distance l (H(2)-H(6)) = 2.206 Å and l (H(13)-O(1)) = 2.307 Å corresponding to the sum of van der Waals radii for these atoms is reached only when the interplane angle is equal to 32.20°.

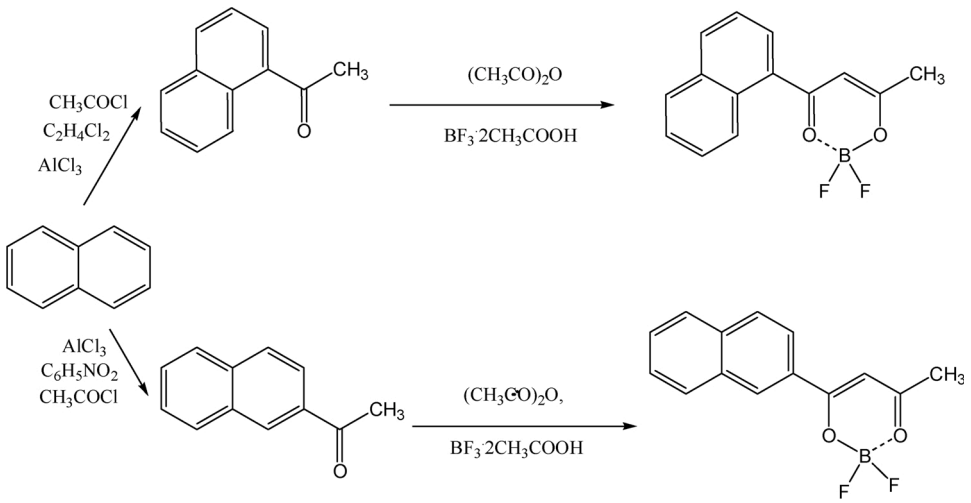
Unlike β-NAcBF$_2$, the difference in bond lengths C(5)-C(6) of the naphthyl group led to the "approaching" and, as a consequence, the repulsion of hydrogen atoms in the molecule of α-NAcBF$_2$ (Table 1). This is a consequence of the difference in bond lengths between carbon atoms in the 1 and 2 positions and in the 2 and 3 positions in the naphthalene molecule (1.369 Å and 1.404 Å, respectively) [51].

3.3. Absorption spectra, electronic structure and luminescence properties of α-NAcBF$_2$ and β-NAcBF$_2$ diluted solutions

The experimental absorption spectra of two isomers differed significantly (Fig. 2a). In the case of α-NAcBF$_2$, the spectrum represented a wide intensive band with a maximum of 367 nm and two less intensive bands in the short-wavelength range. In case of β-NAcBF$_2$, it was an intensive band with a maximum of 343 nm, a band at 380 nm, and two low-intensive bands in the short-wavelength range. Here, the positions of the maxima of the luminescence spectra of the isomers differed insignificantly (Fig. 2b).

Для объяснения наблюдаеМых спектральных особенностей двух изоМеров проведено Моделирование спектров поглощения. In the calculated absorption spectra of the both isomers, the first two bands had proximate positions: 379 nm ($S_0 \rightarrow S_1$) and 317 nm ($S_0 \rightarrow S_2$) for α-NAcBF$_2$; 372 nm ($S_0 \rightarrow S_1$) and 317 nm ($S_0 \rightarrow S_2$) for β-NAcBF$_2$ (Fig. 2a). In the theoretical absorption spectra, positions of the $S_0 \rightarrow S_1$ transition of α-NAcBF$_2$ and β-NAcBF$_2$ are close to each other (Fig. 2a). In the experimental absorption spectra, the intensities of the bands of the $S_0 \rightarrow S_1$ transition differ significantly (Fig. 2a). In the α-NAcBF$_2$ isomer, this band is of maximal intensity, whereas in β-NAcBF$_2$ it is manifested as a long-wavelength shoulder, and the maximal intensity characterizes the band of the $S_0 \rightarrow S_2$ transition. In general, one observes a good agreement between the experimental and theoretical absorption spectra of α-NAcBF$_2$ and β-NAcBF$_2$ isomers (Fig. 2a).

The effect of the torsion angle between the chelate cycle and the naphthyl group (for α-NAcBF$_2$ 34.26°, for β-NAcBF$_2$ 2.13°), which reduced the π-π coupling between two π-systems in the α-NAcBF$_2$ molecule, was displayed in the difference in the electron density distribution on HOMO-1 and the subjacent orbitals. In α-NAcBF$_2$, the electron density on HOMO-1 was fully localized on the naphthyl group (Fig. 3), while in β-NAcBF$_2$ it was delocalized throughout a molecule. Probably, the $S_0 \rightarrow S_2$ (HOMO-1→LUMO) transition in the β-NAcBF$_2$ absorption spectrum has the maximal intensity because of similar distribution of the electron density on HOMO-1 and LUMO and, therefore,



Scheme 2. Synthesis of the isomers α-NAcBF$_2$ (above) and β-NAcBF$_2$ (below).

Table 1
Main bond lengths (Å), torsion angle (°) of α-NAcBF$_2$ and β-NAcBF$_2$.

Bond/angle	Calculated				Experimental	
	α-NAcBF$_2$	α-NAcBF$_2$*	β-NAcBF$_2$	β-NAcBF$_2$*	α-NAcBF$_2$	β-NAcBF$_2$
C(2)-C(1) **	1.402	1.411	1.402	1.393	1.371(4)	1.377(4)
C(2)-C(3)	1.391	1.387	1.391	1.393	1.370(4)	1.365(4)
C(1)-C(5)	1.478	1.468	1.475	1.471	1.460(4)	1.463(4)
O(1)-C(1)	1.290	1.320	1.293	1.327	1.300(3)	1.302(3)
O(2)-C(3)	1.290	1.304	1.289	1.315	1.283(4)	1.303(3)
C(5)-C(6)	1.386	1.423	1.425	1.405	1.376(4)	1.414(4)
∠O(1)C(1)C(5)C(10)	39.02	0.0	9.95	2.54	32.20	2.13

* Optimized geometry in the excited state.
** Atom numbers are shown on the scheme.

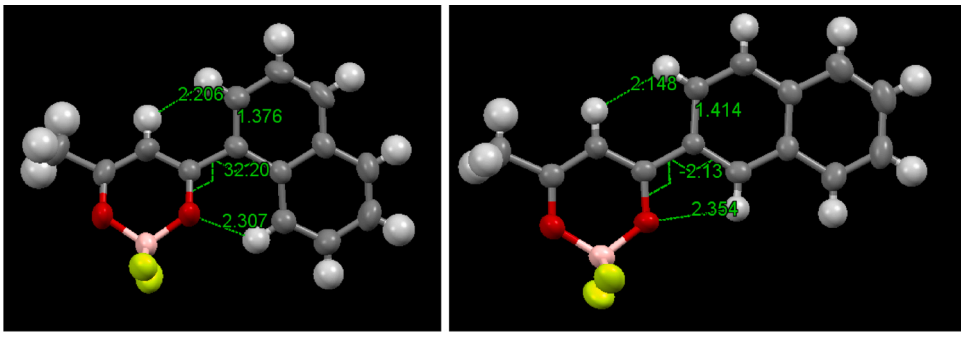


Fig. 1. Structure of the α-NAcBF$_2$ (left) and β-NAcBF$_2$ (right) molecules.

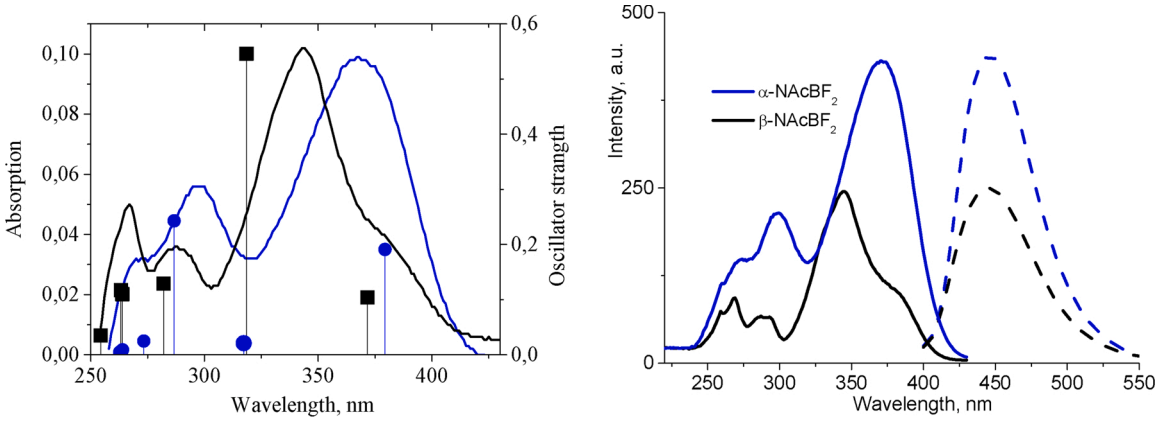


Fig. 2. Spectra of α-NAcBF$_2$ and β-NAcBF$_2$ in chloroform: (a) – theoretical absorption spectra α-NAcBF$_2$ ((blue circles) and β-NAcBF$_2$ (black squares) and experimental absorption spectra of α-NAcBF$_2$ (blue line) and β-NAcBF$_2$ (black line); (b) – excitation spectra (solid line) for α-NAcBF$_2$ λ_{reg} =450 nm, for β-NAcBF$_2$ λ_{reg} =450 nm; luminescence spectra (dash line) for α-NAcBF$_2$ λ_{ex} =370 nm, for β-NAcBF$_2$ λ_{reg} =345 nm.

the smallest shift of the electron density during the transition. For α-NAcBF$_2$, as a result, of non-planar structure, this transition was not realized and the maximum intensity was demonstrated by the transition HOMO – LUMO. This determined the difference in the absorption and excitation spectra of the isomers.

In the case of α-NAcBF$_2$, the main channel of the energy absorption is the $S_0 \rightarrow S_1$ transition, and then there occur the vibrational relaxation $S_1 \rightarrow S'_1$ and fluorescence $S'_1 \rightarrow S'_0$. In the case of β-NAcBF$_2$, the main channel of energy absorption is the $S_0 \rightarrow S_2$ transition, and then there occur fast $S_2 \rightarrow S_1$ transition and, further, as in the case of α-NAcBF$_2$, the vibrational relaxation $S_1 \rightarrow S'_1$ and fluorescence $S'_1 \rightarrow S'_0$. Thus, significant differences in the experimental spectra (Fig. 2a) result from different strengths of the oscillator of $S_0 \rightarrow S_2$ transitions, whereas the similarity of the luminescence spectra result from similar values of the energies of $S_1 \rightarrow S_0$ transitions in α-NAcBF$_2$ and β-NAcBF$_2$.

Positive luminescence solvatochromism was observed for both isomers – α-NAcBF$_2$ and β-NAcBF$_2$. As the solvent polarity increased, the Stokes shift increased too, and the quantum yield of luminescence and the lifetime of the excited state increased as well (Fig. 4, Table 2).

These positive solvatochromism properties can be analyzed in terms of the Lippert–Mataga model and the solvent polarity parameter determined by the factor Δf according to Eq. 1, in which ε and n are the dielectric constant and the refractive index of the solvent, respectively. The Stokes shift ($\Delta\nu$) expressed in cm^{-1} is a function of Δf accrording to Eq. 2, where K is a constant, c and h are the light speed and the Planck constant, respectively, a is the radius of the spherical cavity of the solute, and $\Delta\mu$ is the dipole moment difference between the ground and the excited states [52]. Change in the dipole moment derived from the Lippert–Mataga model are equal to 3.2 and 14.2 D for α-NAcBF$_2$ and β-NAcBF$_2$, respectively.

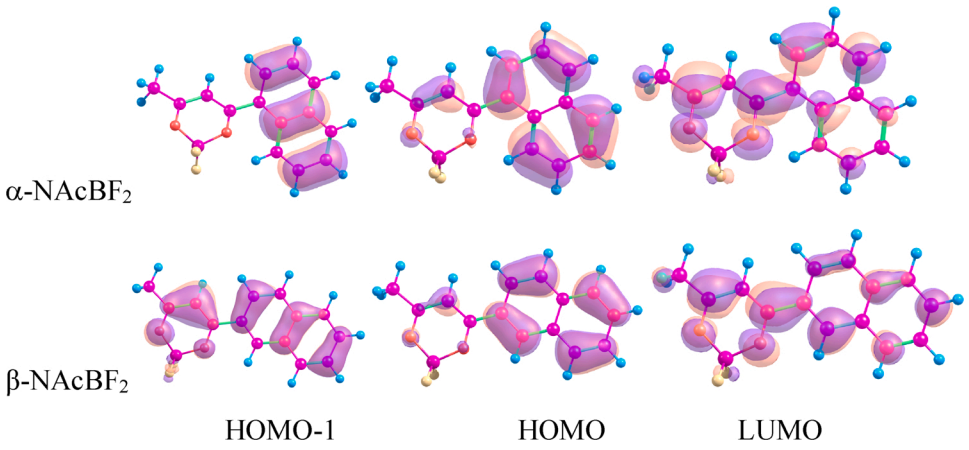


Fig. 3. Molecular orbitals of α-$NAcBF_2$ and β-$NAcBF_2$.

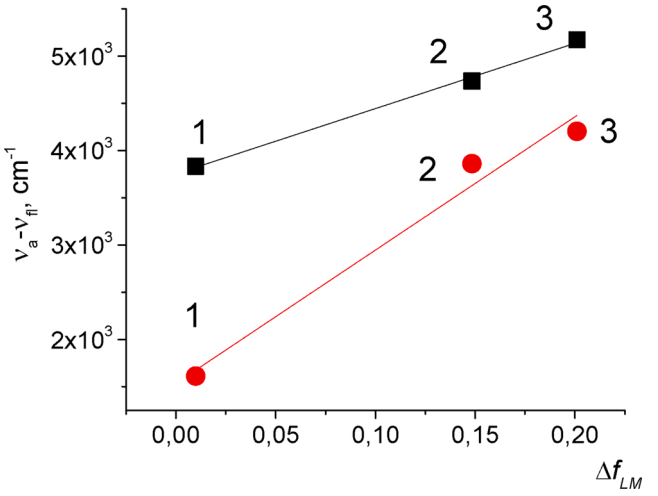


Fig. 4. Lippert–Mataga plot between f_{LM} (ε, η) vs. ($\nu_a - \nu_f$) cm^{-1} for the compounds α-$NAcBF_2$ (square) and β-$NAcBF_2$ (cycle); solvents: 1 – carbon tetrachloride, 2 – chloroform, 3 – dichloromethane.

$$\Delta f = \frac{\varepsilon - 1}{2\varepsilon + 1} - \frac{n^2 - 1}{2n^2 + 1} \quad (1)$$

$$\Delta\nu = \frac{2}{hc}\Delta f \frac{\Delta\mu^2}{a^3} + K \quad (2)$$

3.4. Conformers of α-$NAcBF_2$ and β-$NAcBF_2$ in solutions

The calculation predicted the presence of two possible conformations for each of the isomers differing in the position of the naphthyl group (Fig. 5).

For α-$NAcBF_2$, energy difference between conformations **A** and **B** (Fig. 5) equaled to 0.9 kcal/mol, for β-$NAcBF_2$ – 0.08 kcal/mol. To calculate the transition energy between the conformations **A** and **B**, total energy of the molecule was determined at a perpendicular arrangement of the naphthyl group and the diketonate cycle (**AB**). For α-$NAcBF_2$, the rotation barrier for the C(1)-C(5) bond linking the naphthyl group to the diketonate cycle equaled to 3.5 kcal/mol for **A** and **B** in the ground state, and to 7 kcal/mol for the **A** conformation, and 4 kcal/mol for the **B** one in the excited state (Fig. 6a). Accordingly, the rotation barrier for β-$NAcBF_2$ for **A** and **B** in the ground state equaled to 6.6 kcal/mol, while in the excited state it was 10 kcal/mol (Fig. 6b). In the ground state, the transition between **A** and **B** conformations is possible for both isomers. In the excited state for α-$NAcBF_2$, the transition from the **B** conformation to the more energy-efficient **A** conformation is more probable, whereas in case of β-$NAcBF_2$ the transition between conformations is hampered due to high value of the energy barrier.

For β-$NAcBF_2$, as for a number of other β-diketonates of boron difluoride [56], in the geometry of the excited relaxed state, the molecule remained planar, and there was observed a decrease in the bond length of C(1)-C(5) from 1.475 to 1.471 Å (conformation **A**) and from 1.475 to 1.468 Å (conformation **B**) (Fig. 5). Here, in the β-diketonate cycle, the C—O bond lengths increased, and the C(1)-C(2) and C(2)-C(3) bond lengths leveled (Table 1). The calculated value of λ_{abs} =372 nm, λ_{lum} =421 nm (conformation **A**) and λ_{abs} =370 nm, λ_{lum} =418 nm (conformation **B**), which complied with the experimental data (Table 2). For β-$NAcBF_2$, the existence of both conformers in the ground and excited states is equally probable, but the transition between conformers occurs in the ground state. The absorption and luminescence spectra are contributed by both conformers, the differences between the bands of **A** and **B** conformers in the calculated spectra are insignificant (2–3 nm), and individual bands are not observed in the experimental spectra.

For α-$NAcBF_2$, the pattern was more complex. The repulsion between hydrogen atoms, which resulted in a non-planar structure of the molecule already in the ground state, prevented the length reduction of the C—C bond between the naphthyl group and the diketonate cycle, which was typical for boron difluoride β-diketonates [57]. Here, the values λ_{max} of the luminescence spectra of α-$NAcBF_2$ and β-$NAcBF_2$ were similar (Table 2) and within the range 420–460 nm depending on the

Table 2
Spectral properties of the solutions of α-$NAcBF_2$ and β-$NAcBF_2$.

Compound	Solvent	λ^*_{abs}, nm	$\Delta\nu_{ST}$, cm^{-1}	λ_{lum}, nm	ϕ	τ, ns	k_{fl}	k_{nr}
α-$NAcBF_2$	CH_2Cl_2	367	5173	453	0.55	8.5	$6.5\cdot10^7$	$5.2\cdot10^7$
	$CHCl_3$	367	4736	445	0.68	4.6	$1.5\cdot10^8$	$7.0\cdot10^7$
	CCl_4	361	3834	419, 436	0.17	1.4	$1.21\cdot10^8$	$5.8\cdot10^8$
β-$NAcBF_2$	CH_2Cl_2	343, 379	4203	457	0.38	10.0	$3.8\cdot10^7$	$6.2\cdot10^7$
	$CHCl_3$	343, 379	3862	444	0.37	7.1	$5.2\cdot10^7$	$8.8\cdot10^7$
	CCl_4	341, 374	1612	398, 419	0.15	1.8	$8.3\cdot10^7$	$4.7\cdot10^8$

* The position of the maximum of the long-wave absorption band of β-$NAcBF_2$ was calculated using the spectrum deconvolution by the Gauss functions (Fig. 8S).

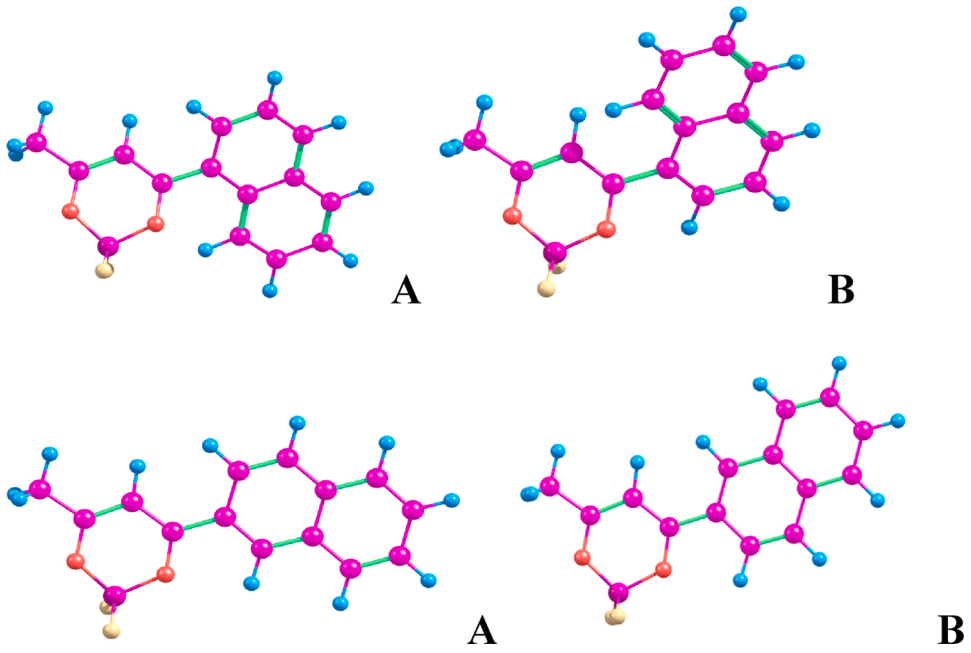


Fig. 5. Conformations of α-NAcBF$_2$ (below) and β-NAcBF$_2$ (above). The "**A**" indicates a more favorable conformation.

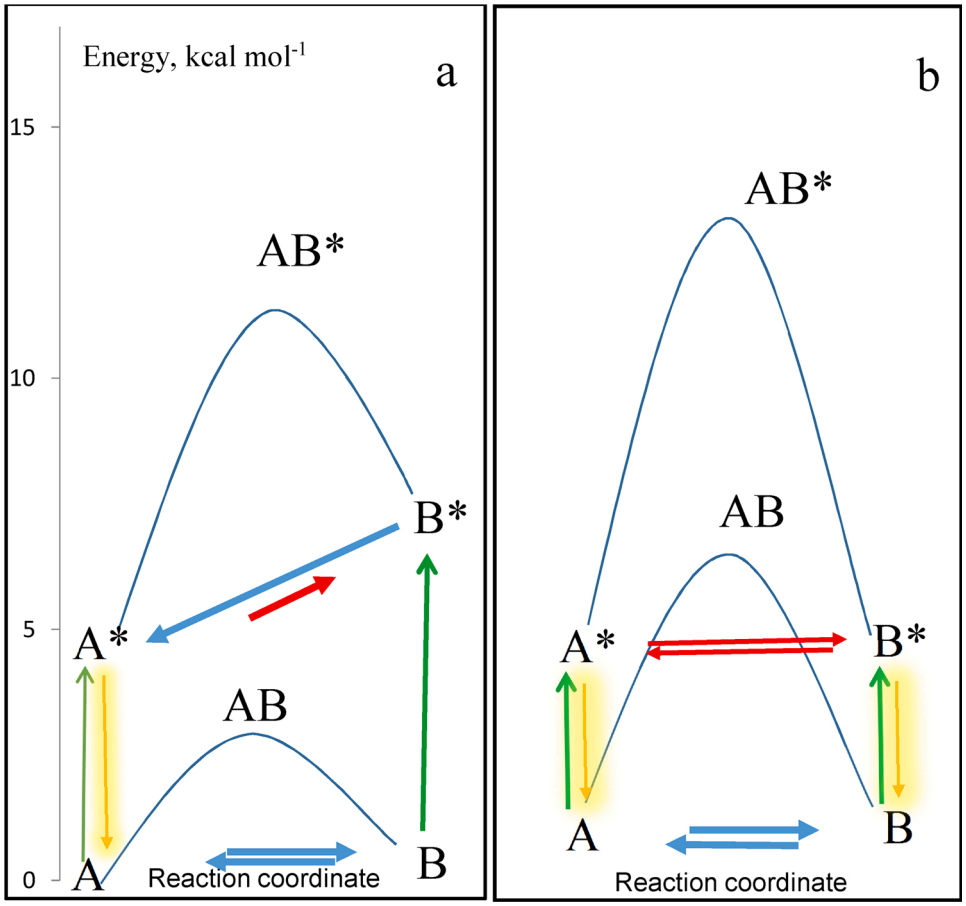


Fig. 6. Relative energies with respect to the ground state of α-NAcBF$_2$ **(A)** of the conformations in ground and excited relaxed states: (a) - α-NAcBF$_2$, (b) – β-NAcBF$_2$. Green arrow – absorption, yellow arrow – luminescence, blue arrow – transition between conformations **A** and **B**, red arrow – energetically uneffective transition between conformations **A** and **B.**

solvent. Similarity of the luminescence spectra of α-$NAcBF_2$ and β-$NAcBF_2$ must be determined by similar locations of the electron density at the frontier orbitals and the geometric structure of the molecules in the relaxed excited state. In case of the conformation A for α-$NAcBF_2$, during relaxation, the diketonate and naphthyl fragments of the molecule were located in the same plane, the C—C bond length between them decreased from 1.476 to 1.462 Å (Table 1), while the C—C bond lengths of the naphthyl fragment increased (Fig. 14S). For the conformation **A**, the calculated value of λ_{abs}=379 nm, λ_{lum} =429 nm, which complied with the experimental value (Table 2). For the conformation **B**, the calculated value of λ_{lum} =366 nm, λ_{lum} =402 nm differed significantly from the experimental one (Table 2), while during relaxation the length of the C—C bond between the diketonate and naphthyl fragments increased up to 1.498 Å (Fig. 14S). The value of total energy for the conformation **B** in the excited relaxed state was higher, and the value of the energy barrier during rotation was lower than for the conformation **A** (Fig. 6a).

To sum up, in case of α-$NAcBF_2$ in the ground state, the existence of **A** and **B** conformers is equally probable, and the transition between them is possible. In the excited state, the existence of **A** conformers and the transition from **B*** to **A*** ones are more energy-efficient. Therefore, the luminescence of α-$NAcBF_2$ is predominantly the emission of conformation **A**.

Rotation of the aromatic α-substituent is known to be one of the main channels of dissipation of the energy of electronic excitation of boron difluoride β-diketonates [53–55]. Those very high-energy values of the rotation barriers in the excited state caused high quantum yield and long lifetime of the excited state of α-$NAcBF_2$ and β-$NAcBF_2$ (Table 2).

3.5. *Luminescence properties of α-$NAcBF_2$ and β-$NAcBF_2$ crystals*

Despite the similarity of the luminescence properties of the solutions of α-$NAcBF_2$ and β-$NAcBF_2$ (Table 2), the properties of their crystals differ significantly (Table 3): crystals of α-$NAcBF_2$ were colorless with intensive blue luminescence (λ_{max}=452 nm, τ = 1.7 ns) β-$NAcBF_2$ – light yellow crystals with yellow-green luminescence (λ_{max}=537 nm, τ = 33.0 ns). For both isomers, the maximum of the crystal excitation spectrum was bathochromically shifted relatively to the solution spectrum and consisted of a wide band in the monomer absorption region and a narrow intensive band in the long-wave region of the spectrum (Fig. 7).

Earlier, there were observed systems found for boron difluoride β-diketonates, in which the steric factor had a important role in the formation of the luminescence properties of crystals [58,59]. In these works, pairs of isomers or groups of compounds with the same π-electron system were investigated. In one case, an effective excimer luminescence was observed, while, in another case, bright monomeric luminescence was found. As a result of the non-planar structure of a molecule [36,58] or the presence of bulk substituents [59], there were no places in the structure of crystals of the second group that were promising in terms of the formation of excimers.

In the α-$NAcBF_2$ crystal, the molecules were packed in stacks. Most β-diketonates of boron difluoride, for which the crystal structure was determined [60], had antiparallel flat molecules. Most often, a position of the coordination site O_2BF_2 was located on one side or the other of the stack, thus achieving mutual compensation of the dipole moments of neighboring molecules. In case α-$NAcBF_2$, the O_2BF_2 groups were located on one side of the stack, whereas the naphthyl groups were on the other side. Inside the stack, the methyl group of one molecule was bound to the fluorine atom of another molecule by a C-H…F bond, the naphthyl groups of neighboring molecules were arranged in a T-shape, and a C-H…π stacking interaction was observed between them.

Table 3
Spectral data on the crystals and solutions of α-$NAcBF_2$ and β-$NAcBF_2$ in dioxane at 77 K.

Compound	Solution			Crystals		
	λ_{fl}, nm	$\lambda_{del,fl}$, nm	λ_{phos}, nm (τ, ms)	λ_{fl}, nm	$\lambda_{del,fl}$, nm (τ, ms)	λ_{phos}, nm (τ, ms)
α-$NAcBF_2$	420	420	550 (524)	448	463 (33)	598 (210)
β-$NAcBF_2$	420	–	527, 565 (98)	530	527 (8)	607, 667 (17)

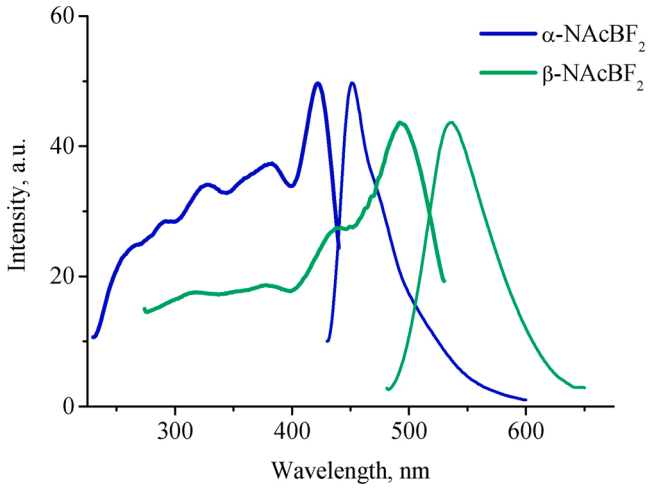


Fig. 7. Excitation (left) and luminescence (right) spectra of crystals α-$NAcBF_2$ and β-$NAcBF_2$.

In the α-$NAcBF_2$ crystal, along the *b*-axis, one can distinguish a structure that corresponded to the structure of "herringbone" J-aggregates (Fig. 8a). The following spectral data supported the assumption of J-aggregates formation in α-$NAcBF_2$ crystal. For α-$NAcBF_2$ crystals, the position of the maximum of the luminescence spectrum (452 nm) and the lifetime of the excited state (1.7 ns) corresponded to the luminescence of dilute solutions (Fig. 9). Similar pattern: narrow bands in the excitation and luminescence spectra, the coincidence of a luminescence spectrum with a spectrum of the dilute solution was observed for J-aggregates in the single crystals of boron difluoride dibenzoylmethanate [61] and its adduct with benzene [62]. The excitation spectrum had a narrow intense band with a maximum of 422 nm, which was mirror-symmetrical to a narrow luminescence band λ_{max} =452 nm (Fig. 9), which was typical for luminescence spectra of J-aggregates. At the same time, π-π stacking interaction required for the formation of excimers was not observed in the α-$NAcBF_2$ crystals.

A significant facilitation at assignment of crystals luminescence bands is provided by the analysis of spectra of concentrated solutions. In the case of α-$NAcBF_2$, the maxima of the luminescence spectra of saturated and diluted solutions coincide with that of the crystal spectrum (Fig. 9). Here, for the excitation spectra, one observes a noticeable evolution: the intensity of the band of excitation of monomers at 367 nm decreases at transition from the diluted solution to the concentrated one and, further, to the crystal. Here, in the long-wavelength part of the spectrum, there emerges a narrow band at 420 nm, in the spectra of crystals this band becomes the main one (Fig. 9). The band at 420 nm can be attributed to the aggregate excitation. The formation of excimers could serve as one more sign of aggregation. In the luminescence spectrum of the concentrated solution, one observes a long-wavelength shoulder at 500−600 nm. The luminescence decay kinetics are substantially different at registration in the spectrum maximum (450 nm) and around the shoulder (530 nm): at 450 nm – biexponential – τ_1 = 8.8 ns (46.52 %), τ_2 = 1.2 ns (51.48 %); at 530 nm – monoexponential – τ = 10.2 ns (Fig. 15S). The increase of the lifetime of the excited state and the emergence of a new long-wavelength band in the luminescence spectrum constitute the most important characteristics of excimers, whose formation is facilitated by the presence of aggregate in the solution. Thus, in the concentrated solutions of α-$NAcBF_2$, there form

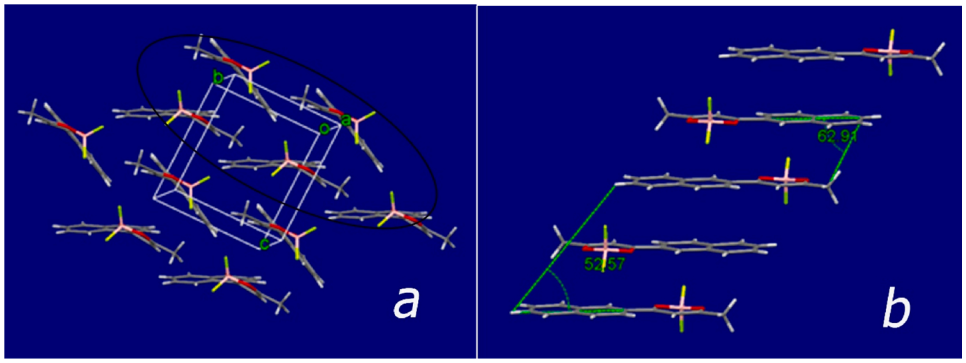


Fig. 8. Structure of J-aggregates in crystals: (a) - α-$NAcBF_2$, (b) - β-$NAcBF_2$.

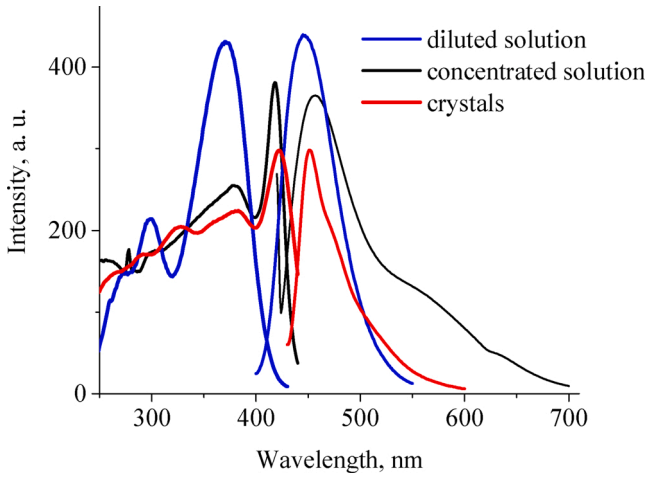


Fig. 9. Excitation (left) and luminescence (right) spectra of α-$NAcBF_2$.

aggregates, with part of them having the excimer luminescence; in crystals, the luminescence of aggregates coincides with that of monomers, π-π stacking interaction required for the formation of excimers was not observed in the α-$NAcBF_2$ crystals.

The excimer nature of luminescence of the concentrated solutions and crystals of β-$NAcBF_2$ was discussed earlier [49,63]. A significant facilitation at assignment of crystals luminescence bands is provided by the analysis of spectra of concentrated solutions. In the case of α-$NAcBF_2$, the maxima of the luminescence spectra of saturated and diluted solutions coincide with that of the crystal spectrum (Fig. 9). Here, for the excitation spectra, one observes a noticeable evolution: the intensity of the band of excitation of monomers at 367 nm decreases at transition from the diluted solution to the concentrated one and, further, to the crystal. Here, in the long-wavelength part of the spectrum, there emerges a narrow band at 420 nm, in the spectra of crystals this band becomes the main one (Fig. 9). The band at 420 nm can be attributed to the aggregate excitation. The formation of excimers could serve as one more sign of aggregation. In the luminescence spectrum of the concentrated solution, one observes a long-wavelength shoulder at 500−600 nm. The luminescence decay kinetics are substantially different at registration in the spectrum maximum (450 nm) and around the shoulder (530 nm): at 450 nm – biexponential – $\tau_1 = 8.8$ ns (46.52 %), $\tau_2 = 1.2$ ns (51.48 %); at 530 nm – monoexponential – $\tau = 10.2$ ns (Fig. 15S). The increase of the lifetime of the excited state and the emergence of a new long-wavelength band in the luminescence spectrum constitute the most important characteristics of excimers, whose formation is facilitated by the presence of aggregate in the solution. Thus, in the concentrated solutions of α-$NAcBF_2$, there form aggregates, with part of them having the excimer luminescence; in crystals, the luminescence of aggregates coincides with that of monomers, π-π stacking interaction required for the formation of excimers was not observed in the α-$NAcBF_2$ crystals.

In the case β-$NAcBF_2$, the evolution of spectra at the transition from diluted solutions to concentrated ones and, further, to crystals differs substantially from that for α-$NAcBF_2$. The maxima of luminescence bands of β-$NAcBF_2$ are bathochromically shifted: 457 nm for the diluted solution, 475 nm for the concentrated one, and 539 nm for crystals (Fig. 10). The maxima of excitation spectra are also bathochromically shifted, whereas the spectra structure changes significantly (Fig. 10). The excitation spectrum of the diluted solution coincides with the absorption spectrum, the band at 343 nm disappears in the spectrum of the concentrated solution, the band at 389 nm remains in the range of monomer excitation, and there emerges a new narrow intensive band at 425 nm, which shifts to 500 nm at the transition to crystals. At the transition from the diluted solution of β-$NAcBF_2$ to the concentrated one, one observes an asymmetry and significant broadening of the luminescence band. Deconvolution of this band on Gauss functions enabled one to reveal the presence of two components with maxima at 460 and 510 nm (Fig. 10). The component at 460 nm corresponds to the luminescence of the diluted solution of β-$NAcBF_2$ at 457 nm. Kinetics of luminescence at 460 nm – biexponential – $\tau_1 = 16.7$ ns (59.13 %), $\tau_2 = 2.7$ ns (40.87 %); kinetics at 510 nm – monoexponential – $\tau = 20.0$ ns (Fig. 16S). Accordingly, the band at 460 nm can be attributed to the monomer luminescence, while the band at 510 nm – to the excimer luminescence.

The maximum of the luminescence spectrum of β-$NAcBF_2$ crystals equaled to 539 nm, the quenching kinetics was monoexponential, $\tau = 33.0$ ns. The large lifetime and significant bathochromic shift of the

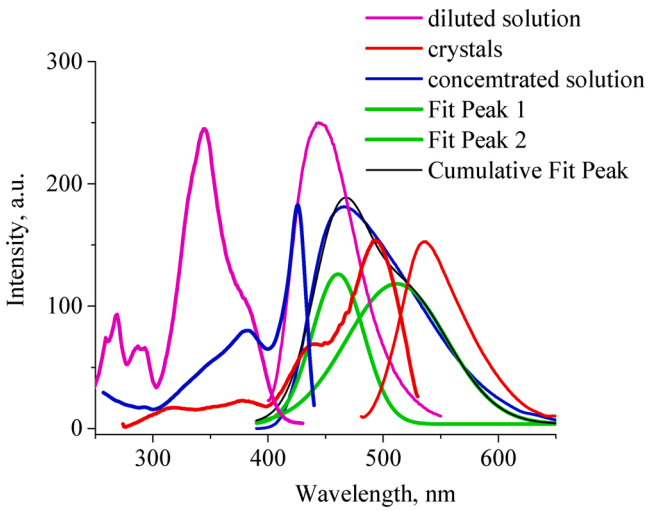


Fig. 10. Excitation (left) and luminescence (right) spectra of β-$NAcBF_2$.

luminescence spectrum relatively to the dilute solution spectrum clearly indicated the excimer luminescence of the β-NAcBF$_2$ crystals.

3.6. Phosphorescence of α-NAcBF$_2$ and β-NAcBF$_2$

The luminescence and phosphorescence spectra for the crystals α-NAcBF$_2$ and β-NAcBF$_2$ and solutions were recorded in dioxane at 77 K (Fig.11). Phosphorescence was observed for all the systems at 77 K. For crystals and solutions of α-NAcBF$_2$, delayed fluorescence was observed in addition to phosphorescence (Fig. 11 a, b). In the case of β-NAcBF$_2$, delayed fluorescence was observed only for the crystals (Fig. 11 b, d).

Quantum chemistry simulation of the NAcBF$_2$ and β-NAcBF$_2$ molecules in the geometry of the ground and excited relaxed states was performed in order to identify the cause of different ways of deactivating the electron excitation energy in the investigated isomers. For α-NAcBF$_2$, unlike β-NAcBF$_2$, there was an inversion observed of the S_1 and T_2 levels during vibrational relaxation from the S_0 geometry to the optimal S_1 geometry, which caused the intersection of potential energy surfaces in the states S_1 and T_2 (Fig. 17S).

In case of α-NAcBF$_2$, inversion of the levels S_1 and T_2 during relaxation from the geometry S_0 into the optimal geometry S_1 promoted population of the T_2 level, phosphorescence along the channel $T_2 \rightarrow T_1 \rightarrow S_0$, and delayed fluorescence along the channel $T_2 \rightarrow S_1 \rightarrow S_0$ (Fig. 12a). Both processes were observed at 77 K in solution and in crystals. As was shown above, the fluorescence of α-NAcBF$_2$crystals was monomeric (452 nm (300 K) and 448, 471 (77 K)), while the delayed fluorescence (λ_{max}=494 nm) of the α-NAcBF$_2$solutions and crystals was monomeric as well.

For β-NAcBF$_2$, the traditional arrangement of the singlet and triplet levels was observed (Fig. 17S). Occupation of the T_2 level proceeded with S_1. Phosphorescence $T_2 \rightarrow T_1 \rightarrow S_0$ was observed for both solutions and crystals. Unlike α-NAcBF$_2$, the delayed fluorescence in the solution of β-NAcBF$_2$ was absent and registered only for crystals (Fig. 11). In the β-NAcBF crystal, molecules are packed as dimers capable to excimer fluorescence. (Fig. 7b). The fluorescence of β-NAcBF$_2$ crystals (530 nm at 300 and 77 K) was an excimer one [49], just like the delayed fluorescence of the crystals (531 nm). The delayed fluorescence of β-NAcBF$_2$ of the P-type occurred as a result of triplet-triplet annihilation with the excimer formation (Fig. 12b) [64]:

$2T^* \rightarrow D^* \rightarrow 2M + h\nu$ (T – triplet, D* – excimer, M – monomer).

One should mention a significantly longer lifetime of phosphorescence of the solutions and crystals of α-NAcBF$_2$ compared to that of β-NAcBF$_2$ (Table 3, Fig. 18 S–21 S). A feature of the structure of the α-NAcBF$_2$ molecule in the relaxed excited state consisted in proximate positions of the levels S_1, T_1, and T_2 (Fig. 17S). This allowed both triplet levels T_1 and T_2 to participate in occupation of the S_1 level, which resulted in intense delayed fluorescence and large life time of phosphorescence.

4. Conclusions

A comparative study of the luminescence properties of solutions and crystals of two isomers has been performed: 1-(1′-naphthyl)butanedionate-1,3 (α-NAcBF$_2$) and 1-(2′-naphthyl)butanedionate-1,3 (β-NAcBF$_2$) of boron difluoride. An interrelation between the molecular and crystal structure of the studied complexes and their luminescent properties has been revealed. Iin the α-NAcBF$_2$ molecule the plane of the naphthyl

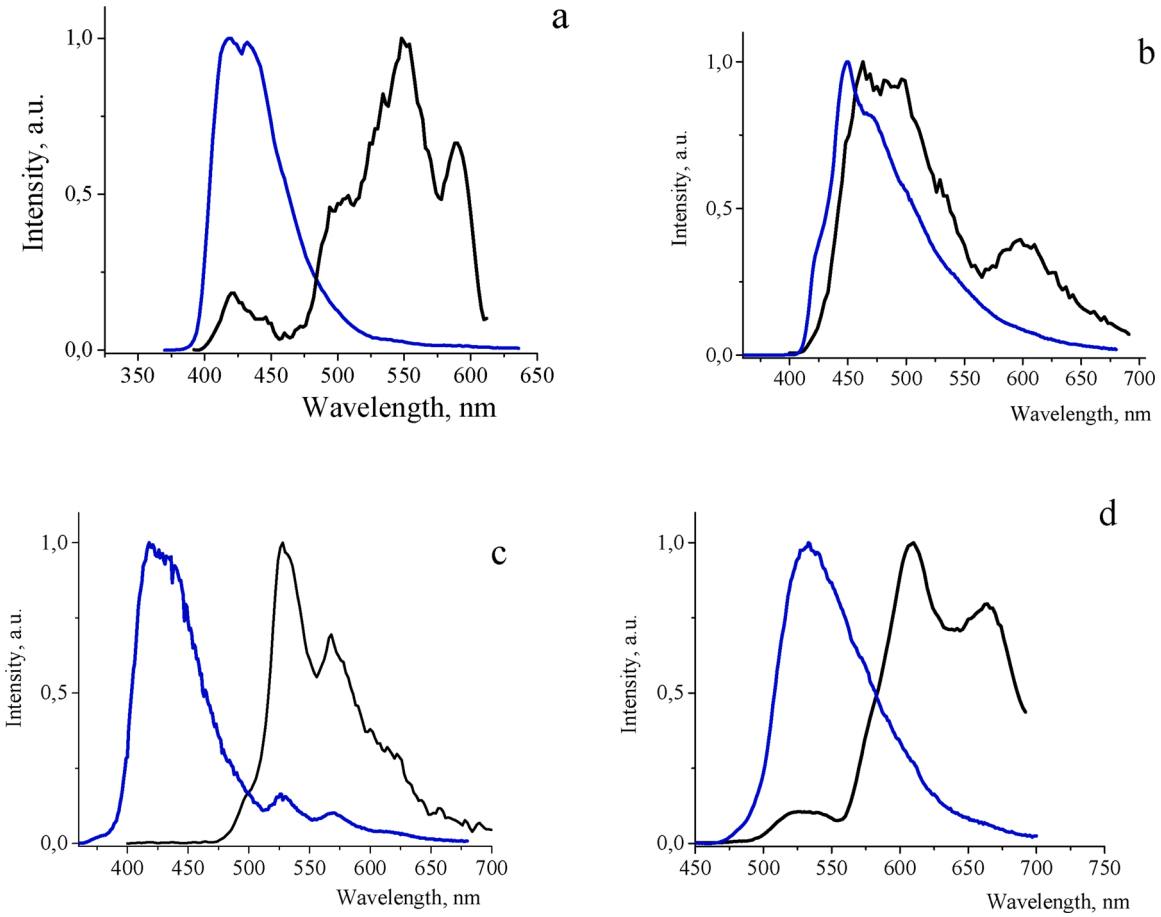


Fig. 11. Luminescence spectra of α-NAcBF$_2$ and β-NAcBF$_2$at 77 K: (a) solution of α-NAcBF$_2$ in dioxane, (b) crystals of α-NAcBF$_2$, (c) solution of β-NAcBF$_2$ in dioxane, (d) crystals of β-NAcBF$_2$. Blue – fluorescence spectrum, black – delay fluorescence and phosphorescence spectrum.

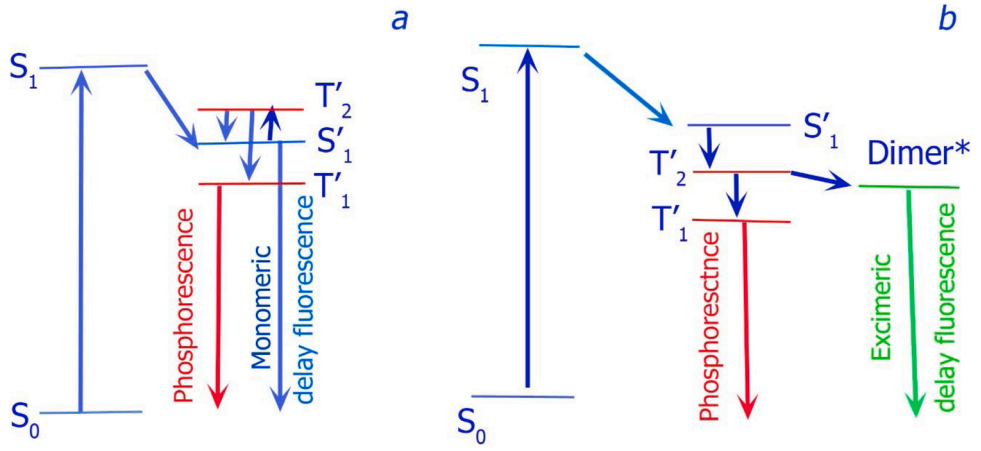


Fig. 12. Diagram of the photophysical processes in (a) α-$NAcBF_2$ and (b) β-$NAcBF_2$.

group was rotated by 34.26° relatively to the chelate cycle, whareas in the β-$NAcBF_2$ planar molecule.

The structures of HOMO and LUMO of α-$NAcBF_2$ and β-$NAcBF_2$ appeared to be similar: for HOMO the electron density is localized on the naphthyl group, while for LUMO it is delocalized throughout a molecule. Differences in the electronic structure of isomers are observed for HOMO-1 and the subjacent orbitals. In α-$NAcBF_2$, the electron density on HOMO-1 is fully localized on the naphthyl group, and in β-$NAcBF_2$ – delocalized throughout a molecule. Similarity of the luminescence spectra is the result of approximate values of the first transition energies of α-$NAcBF_2$ and β-$NAcB_{F2}$

For both isomers, the maximum of the crystal excitation spectrum was bathochromically shifted relatively to the solution spectrum and contained a narrow intensive band in the long-wavelength range of the spectrum corresponding to the J-aggregates excitation. The difference in the luminescent properties of the crystals α-$NAcBF_2$ (452 nm) and β-$NAcBF_2$ (537 nm) is caused by different abilities to form excimers. In β-$NAcBF_2$ crystals, J-aggregates consist of dimers of antiparallel molecules comprising excimer traps. In α-$NAcBF_2$ crystals, the turning of the naphthyl group prevents the formation of dimers, and, in this case, luminescence of only single molecules was observed.

In crystals and solutions of α-$NAcBF_2$ at 77 K, the delayed fluorescence has been observed in addition to phosphorescence. In case of β-$NAcBF_2$, the delayed fluorescence has been detected only for crystals, while phosphorescence – for crystals and solutions. For α-$NAcBF_2$, unlike to β-$NAcBF_2$, there was observed an inversion of the S_1 and T_2 levels at vibrational relaxation from the S_0 geometry into the optimal S_1 geometry, which caused the intersection of potential energy surfaces in the S_1 and T_2 states. A feature of the structure of the α -$NAcBF_2$ molecule in the geometry of the relaxed excited state consists in the proximate positions of the S_1, T_1, and T_2 levels. The latter allows both triplet levels T_1 and T_2 to participate in population of the S_1 level, which results in an intensive delayed fluorescence and extended duration of phosphorescence.

CRediT authorship contribution statement

Elena V. Fedorenko: Investigation, Writing - original draft. **Anatolii G. Mirochnik:** Investigation, Writing - review & editing. **Andrey V. Gerasimenko:** Investigation. **Anton Yu. Beloliptsev:** Investigation. **Zakhar N. Puzyrkov:** Investigation. **Irina V. Svistunova:** Investigation. **Aleksander A. Sergeev:** Investigation.

Declaration of Competing Interest

The authors report no declarations of interest.

Acknowledgments

The research was performed with a support of the Russian Foundation for Basic Research (Project No. 19-03-00409).

The authors are grateful to the Far Eastern Centre of Structural Research for performing the X-ray investigation.

Appendix A. Supplementary data

Supplementary material related to this article can be found, in the online version, at doi:https://doi.org/10.1016/j.jphotochem.2021.113220.

References

[1] L.D. Lavis, R.T. Raines, Bright building blocks for chemical biology, ACS Chem. Biol. 9 (2014) 855–866, https://doi.org/10.1021/cb500078u.
[2] E.C. Stack, C. Wang, K.A. Roman, C.C. Hoyt, Multiplexed immunohistochemistry, imaging, and quantitation: a review, with an assessment of Tyramide signal amplification, multispectral imaging and multiplex analysis, Methods 70 (2014) 46–58, https://doi.org/10.1016/j.ymeth.2014.08.016.
[3] U. Resch-Genger, M. Grabolle, S. Cavaliere-Jaricot, R. Nitschke, T. Nann, Quantum dots versus organic dyes as fluorescent labels, Nat. Methods 5 (2008) 763–775, https://doi.org/10.1038/nmeth.1248.
[4] K. Ariga, T. Mori, J.P. Hill, Mechanical control of nanomaterials and nanosystems, Adv. Mater. 24 (2012) 158–176, https://doi.org/10.1002/adma.201102617.
[5] B. Xu, Z. Chi, X. Zhang, H. Li, C. Chen, S. Liu, Y. Zhanga, J. Xu, A new ligand and its complex with multi-stimuli-responsive and aggregation-induced emission effects, Chem. Commun. (Camb.) 47 (2011) 11080–11082, https://doi.org/10.1039/C1CC13790E.
[6] Y. Gong, Y. Tan, J. Liu, P. Lu, C. Feng, W.Z. Yuan, Y. Lu, J.Z. Sun, G. He, Y. Zhang, Twisted D–π–a solid emitters: efficient emission and high contrast mechanochromism, Chem. Commun. (Camb.) 49 (2013) 4009–4011, https://doi.org/10.1039/C3CC39243K.
[7] W.L. Rumsey, J.M. Vanderkooi, D.F. Wilson, Imaging of phosphorescence: a novel method for measuring oxygen distribution in perfused tissue, Science 241 (1988) 1649–1651, https://doi.org/10.1126/science.342041.
[8] M. Sinaasappel, C. Ince, Calibration of Pd-porphyrin phosphorescence for oxygen concentration measurements in vivo, J. Appl. Physiol. 81 (1996) 2297–2303, https://doi.org/10.1152/jappl.1996.81.5.2297.
[9] N. Boens, V. Leen, W. Dehaen, Erratum: Fluorescent indicators based on BODIPY, Chem. Soc. Rev. 41 (2012) 1130–1172, https://doi.org/10.1039/c1cs15132k.
[10] A. Loudet, K. Burgess, BODIPY dyes and their derivatives: syntheses and spectroscopic properties, Chem. Rev. 107 (2007) 4891–4932, https://doi.org/10.1021/cr078381n.
[11] Z. Liu, Z. Jiang, M. Yan, X. Wang, Recent progress of BODIPY dyes with aggregation-induced emission, Front. Chem. 7 (2019) 712, https://doi.org/10.3389/fchem.2019.00712.
[12] F. Bergström, I. Mikhalyov, P. Hägglöf, R. Wortmann, T.N. Johansson, B. A. Johansson, Dimers of dipyrromethene boron difluoride (BODIPY) with light spectroscopic applications in chemistry and biology, J. Am. Chem. Soc. 124 (2002) 196–204, https://doi.org/10.1021/ja010983f.
[13] S. Chibani, A. Charaf-Eddin, B. Mennucci, B. Guennic, D. Jacquemin, On the computation of adiabatic energies in aza-boron-dipyrromethene dyes, J. Chem. Theory Comput. 10 (2014) 805–815, https://doi.org/10.1021/ct300618j.
[14] R. Yoshii, A. Nagai, K. Tanaka, Y. Chujo, Boron-ketoiminate-based polymers: fine-tuning of the emission color and expression of strong emission both in the solution

and film states, Macromol. Rapid Commun. 35 (2014) 1315–1319, https://doi.org/10.1002/marc.201400198.
[15] R. Yoshii, K. Tanaka, Y. Chujo, Conjugated polymers based on tautomeric units: regulation of main-chain conjugation and expression of aggregation induced emission property via boron-complexation, Macromolecules 47 (2014) 2268–2278, https://doi.org/10.1021/ma500082e.
[16] R. Yoshii, A. Hirose, K. Tanaka, Y. Chujo, Functionalization of boron diiminates with unique optical properties: multicolor tuning of crystallization-induced emission and introduction into the main chain of conjugated polymers, J. Am. Chem. Soc. 136 (2014) 18131–18139, https://doi.org/10.1021/ja510985v.
[17] R. Yoshii, A. Nagai, K. Tanaka, Y. Chujo, Highly emissive boron ketoiminate derivatives as a new class of aggregation-induced emission fluorophores, Chem. Eur. J. 19 (2013) 4506–4512, https://doi.org/10.1002/chem.201203703.
[18] Y. Kubota, S. Tanaka, K. Funabiki, K. Funabiki, M. Matsui, Synthesis and fluorescence properties of thiazole–boron complexes bearing a β-ketoiminate ligand, Org. Lett. 15 (2013) 1768–1771, https://doi.org/10.1021/ol302179r.
[19] K. Perumal, J.A. Garg, O. Blacque, R. Saiganesh, S. Kaliban, K.K. Balasubramanian, K. Venkatesan, β-Iminoenamine-BF_2 complexes: aggregation-induced emission and pronounced effects of aliphatic rings on radiationless deactivation, Chem. Asian J. 7 (2012) 2670–2677, https://doi.org/10.1002/asia.201200477.
[20] J.F. Araneda, W.E. Piers, B. Heyne, M. Parvez, R. McDonald, High Stokes shift anilido-pyridine boron difluoride dyes, Angew. Chem., Int. Ed. 50 (2011) 12214–12217, https://doi.org/10.1002/anie.201105228.
[21] C. Ran, X. Xu, S.B. Raymond, B.J. Ferrara, K. Neal, B.J. Bacskai, Z. Medarova, A. Moore, Design, synthesis, and testing of difluoroboron-derivatized curcumins as near-infrared probes for in vivo detection of amyloid-β deposits, J. Am. Chem. Soc. 131 (2009) 15257–15261, https://doi.org/10.1021/ja9047043.
[22] M. Koch, K. Perumal, O. Blacque, J.A. Garg, R. Saiganesh, S. Kabilan, K. K. Balasubramanian, K. Venkatesan, Metal-free triplet phosphors with high emission efficiency and high tenability, Angew Chem. Int Ed. 126 (2014) 6496–6500, https://doi.org/10.1002/anie.201402199.
[23] A.G. Mirochnik, E.V. Fedorenko, V.G. Kuryavyi, B.V. Bukvetskii, V.E. Karasev, Luminescence and reversible luminescence thermochromism of bulk and microcrystals of dibenzoylmethanatoboron difluoride, J. Fluoresc. 16 (2006) 279–286, https://doi.org/10.1007/s10895-005-0039-7.
[24] A.G. Mirochnik, E.V. Fedorenko, T.A. Kaidalova, E.B. Merkulov, V.G. Kuryavyi, K. N. Galkin, V.E. Karasev, Reversible luminescence thermochromism and phase transition in crystals of thiophenylacetylacetonatoboron difluoride, J. Lumin. 11 (2008) 1799–1802, https://doi.org/10.1016/j.jlumin.2008.04.016.
[25] A. Sakai, M. Tanaka, E. Ohta, Y. Yoshimoto, K. Mizuno, H. Ikeda, White light emission from a single component system: remarkable concentration effects on the fluorescence of 1,3-diaroylmethanatoboron difluoride, Tetrahedron Lett. 53 (2012) 4138–4141, https://doi.org/10.1016/j.tetlet.2012.05.122.
[26] Y.N. Kononevich, V.A. Sazhnikov, A.S. Belova, A.A. Korlyukov, A.D. Volodin, A. A. Safonov, G.A. Yurasik, D.S. Ionov, A.M. Muzafarov, Turn-on exciplex fluorescence induced by complexation of nonfluorescent pentafluorinated dibenzoylmethanatoboron difluoride with benzene and its derivatives, New J. Chem. 43 (2019) 13725–13734, https://doi.org/10.1039/C9NJ03722E.
[27] A.G. Mirochnik, B.V. Bukvetskii, E.V. Fedorenko, V.E. Karasev, Crystal structures and excimer fluorescence of anisoylbenzoylmethanatoboron and dianisoylmethanatoboron difluorides, Russ. Chem. Bull. 53 (2004) 291–296, https://doi.org/10.1023/B:RUCB.0000030800.71663.7a.
[28] E.V. Fedorenko, B.V. Bukvetskii, A.G. Mirochnik, D.H. Shlyk, M.V. Tkacheva, A. A. Karpenko, Luminescence and crystal structure of 2,2-difluoro-4-(9-anthracyl)-6-methyl-1,3,2-dioxaborine, J. Lumin. 130 (2010) 756–761, https://doi.org/10.1016/j.jlumin.2009.11.027.
[29] Y.L. Chow, C.I. Johansson, Exciplex binding energy and kinetic rate constants of the interaction between singlet excited state (dibenzoylmethanato)boron difluoride and substituted benzenes, J. Phys. Chem. 99 (1995) 17566–17572, https://doi.org/10.1021/j100049a016.
[30] A.A. Safonov, A.A. Bagaturyants, V.A. Sazhnikov, Structures and binding energies of the (dibenzoylmethanato)boron difluoride complexes with aromatic hydrocarbons in the ground and excited states. Density functional theory calculations, High Energy Chem. 48 (2014) 43–48, https://doi.org/10.1134/S0018143914010111.
[31] S. Xu, R.E. Evans, T. Liu, G. Zhang, J.N. Demas, C.O. Trindle, C.L. Fraser, Aromatic difluoroboron β-diketonate complexes: effects of π-conjugation and media on optical properties, Inorg. Chem. 52 (2013) 3597–3610, https://doi.org/10.1021/ic300077g.
[32] C.A. DeRosa, C. Kerr, Z. Fan, M. Kolpaczynska, A.S. Mathew, R.E. Evans, G. Zhang, C.L. Fraser, Tailoring oxygen sensitivity with halide substitution in difluoroboron dibenzoylmethane polylactide materials, ACS Appl. Mater. Interfaces 7 (2015) 23633–23643, https://doi.org/10.1021/acsami.5b07126.
[33] C.A. Derosa, J. Samonina-Kosicka, Z. Fan, H.C. Hendargo, D.H. Weitzel, G. M. Palmer, C.L. Fraser, Oxygen sensing difluoroboron dinaphthoylmethane polylactide, Macromolecules 48 (2015) 2967–2977, https://doi.org/10.1021/acs.macromol.5b00394.
[34] J. Samonina-Kosicka, C.A. Derosa, W.A. Morris, Z. Fan, C.L. Fraser, Dual-emissive difluoroboron naphthyl-phenyl β-diketonate polylactide materials: effects of heavy atom placement and polymer molecular weight, Macromolecules 47 (2014) 3736–3746, https://doi.org/10.1021/ma5006606.
[35] G. Zhang, G.M. Palmer, M.W. Dewhirst, C.L. Fraser, A dual-emissive-materials design concept enables tumour hypoxia imaging, Nat. Mater. 8 (2009) 747–751, https://doi.org/10.1038/nmat2509.
[36] E.V. Fedorenko, B.V. Bukvetskii, A.G. Mirochnik, T.B. Emelina, V.E. Karasev, Influence of the steric effect on the spectral properties of benzoylacetonatoboron difluorides, Russ. Chem. Bull. 58 (2009) 2240–2245, https://doi.org/10.1007/s11172-009-0312-z.
[37] B.V. Bukvetskii, E.V. Fedorenko, A.G. Mirochnik, A. Yu, Beloliptsev, Crystal structure and luminescence of 2,2-difluoro-4,6-(4-methylphenyl)-1,3,2-dioxaborine, J. Struct. Chem. 53 (2012) 73–81, https://doi.org/10.1134/S002247661201009X.
[38] A.G. Mirochnik, B.V. Bukvetskii, E.V. Gukhman, V.E. Karasev, Crystal structure and excimer fluorescence of some benzoylacetonatoboron difluorides: stacking factor, J. Fluoresc. 13 (2003) 157–162, https://doi.org/10.1023/A:1022939209971.
[39] P. Zhang, A.J.J. Kragt, A.P.H.J. Schenning, L.T. Haan, G. Zhou, An easily coatable temperature responsive cholesteric liquid crystal oligomer for making structural colour patterns, J. Mater. Chem. 6 (2018) 7184–7187, https://doi.org/10.1039/C8TC02252F.
[40] M. Pfletscher, C. Wölper, J.S. Gutmann, M. Mezger, M. Giese, Amodular approach towards functional supramolecular aggregates - subtle structural differences inducing liquid crystallinity, Chem. Commun. (Camb.) 52 (2016) 5849–5852, https://doi.org/10.1039/C6CC03966A.
[41] J. Wang, Y. Shi, K. Yang, J. Wei, J. Guo, Stabilization and optical switching of liquid crystal blue phase doped with azobenzene-based bent-shaped hydrogen-bonded assemblies, RSC Adv. 5 (2015) 67357–67364, https://doi.org/10.1039/C5RA12256B.
[42] L. Wang, K.G. Gutierrez-Cuevas, H.K. Bisoyi, J. Xiang, G. Singh, R.S. Zola, S. Kumar, O.D. Lavrentovich, A. Urbasd, Q. Li, NIR light-directing self-organized 3D photonic superstructures loaded with anisotropic plasmonic hybrid nanorods, Chem. Commun. (Camb.) 51 (2015) 15039–15042, https://doi.org/10.1039/C5CC06146F.
[43] N. Donaldson, in: E. Arnold (Ed.), The Chemistry and Technology of Naphthalene Compounds, first ed., 1958. London.
[44] M.W. Schmidt, K.K. Baldridge, J.A. Boatz, S.T. Elbert, M.S. Gordon, J.H. Jensen, S. Koseki, N. Matsunaga, K.A. Nguyen, S.J. Su, T.L. Windus, M. Dupius, J. A. Montgomery, General atomic and molecular electronic-structure system, J. Comp. Chem. 14 (1993) 1347–1363.
[45] A.D. Becke, Density-functional thermochemistry. III. The role of exact exchange, J. Chem. Phys. 98 (1993) 5648–5652.
[46] Bruker, Apex2, Bruker AXS Inc., Madison, WI, USA, 2012.
[47] G.M. Sheldrick, SHELXT – integrated space-group and crystal-structure determination, Acta Cryst 71 (2015) 3–8, https://doi.org/10.1107/S2053273314026370.
[48] G.M. Sheldrick, Crystal structure refinement with SHELXL, Acta Cryst. C 71 (2015) 3–8, https://doi.org/10.1107/S2053229614024218.
[49] B.V. Bukvetskii, E.V. Fedorenko, A.G. Mirochnik, A. Yu, Beloliptsev, Crystal structure of boron difluoride 1-naphthylbutanedionate-1,3 ($C_{10}H_7COCHCOCH_3BF_2$). π-stacking interaction and luminescence, J. Struct. Chem. 51 (2010) 545–551, https://doi.org/10.1007/s10947-010-0079-y.
[50] G. Görlitz, H. Hartmann, B. Nuber, J.J. Wolff, A simple route to 4-aryl and 4-hetaryl substituted 6-methyl-2,2-difluoro-1,3,2-(2h)-dioxaborines, Adv. Synth. Cat. 341 (1999) 167–172, https://doi.org/10.1002/(SICI)1521-3897(199902)341:23.0.CO;2-A.
[51] F.R. Ahmed, D.W.J. Cruickshank, A refinement of the crystal and molecular structures of naphthalene and anthracene, Acta Cryst. 5 (1952) 852–853, https://doi.org/10.1107/S0365110X52002379.
[52] J.R. Lakowicz, Principles of Fluorescence Spectroscopy, 3th ed., Springer Science Business Media, New York, 2006.
[53] K. Gustav, M. Storch, Nichtradiation Desactivierung Von Molekulen; Teoretische Bestimmung der IC- und ISC-Akzeptormoden in ausgewahlten borchelaten, Z. Chem. 28 (1988) 406–408.
[54] K. Gustav, M. Storch, Nicht-radiation Desactivierung Von Molekulen: III. Teoretische Bestimmung der inner konversion von ausgewahlten 1,3-Diketonato-Borkomplexen unter berucksichtigung des akzeptor- und promotorverhaltens, Monatsh. Chim. 121 (1990) 447–454, https://doi.org/10.1007/BF00810851.
[55] G. Haucke, P. Czerney, H.-D. Ilge, D. Steen, H. Hartmann, The effect on internal rotation on absorbtion and fluorescence of dye molecules, J. Mol. Struct. 219 (1990) 411–416, https://doi.org/10.1016/0022-2860(90)80090-7.
[56] E.V. Fedorenko, A.G. Mirochnik, A.Yu. Beloliptsev, I.V. Svistunova, G. O. Tretyakova, Synthesis, molecular design and crystallization-induced emission of novel boron difluorides β-ketoiminates, ChemPlusChem. 83 (2018) 117–127, https://doi.org/10.1002/cplu.201800069.
[57] S.A. Tikhonov, E.V. Fedorenko, A.G. Mirochnik, I.S. Osmushko, A.D. Skitnevskaya, A.B. Trofimov, V.I. Vovna, Spectroscopic and quantum chemical study of difluoroboron β-diketonate luminophores: isomeric acetylnaphtholate chelates, Spectrochim. Acta A. 214 (2019) 67–78, https://doi.org/10.1016/j.saa.2019.02.002.
[58] P. Galer, R.C. Korosec, M. Vidmar, B. Sket, Crystal structures and emission properties of the bf_2 complex 1-phenyl-3-(3,5-dimethoxyphenyl)-propane-1,3-dione: multiple chromisms, aggregation- or crystallization-induced emission, and the self-assembly effect, J. Am. Chem. Soc. 136 (2014) 7383–7394, https://doi.org/10.1021/ja501977a.
[59] A. Sakai, E. Ohta, Y. Yoshimoto, M. Tanaka, Y. Matsui, K. Mizuno, H. Ikeda, New fluorescence domain “excited multimer” formed upon photoexcitation of continuously stacked diaroylmethanatoboron difluoride molecules with fused p-orbitals in crystals, Chem. Eur. J. 21 (2015) 18128–18137, https://doi.org/10.1002/chem.201503132.
[60] C.R. Groom, F.H. Allen, The cambridge structural database in retrospect and prospect, Angew. Chem. Int. Ed. 53 (2014) 662–671, https://doi.org/10.1002/anie.201306438.

[61] A.G. Mirochnik, E.V. Fedorenko, A.A. Karpenko, D.A. Gizzatulina, V.E. Karasev, Size-dependent fluorescence of dibenzoylmethanate and ditoluylmethanate of boron difluoride, Lumines. 22 (2007) 195–198, https://doi.org/10.1002/bio.948.
[62] E.V. Fedorenko, A.G. Mirochnik, I.B. Lvov, V.I. Vovna, Luminescence of solvate boron difluoride dibenzoylmethanate with benzene: Aggregates formation, Sectrochim. Acta A. 120 (2014) 119–125, https://doi.org/10.1016/j.saa.2013.10.016.
[63] E.V. Fedorenko, A.G. Mirochnik, A.Yu. Beloliptsev, Molecular design and luminescence of boron difluoride benzoylacetonates, J. Lumin. Appl. 196 (2018) 316–325, https://doi.org/10.1016/j.jlumin.2017.12.071.
[64] B. Ranby, J.B. Rabek, Photodegradation, Photo-oxidation and Photostabilization of Polymers. Principles and Applications, John Wiley & Sons Inc, London, 1975.